UDK 536.421.5:666.11
Original scientific article/Izvirni znanstveni članek

ISSN 1580-2949
Mater. Tehnol.

STUDY ON THE EFFECT OF SINTERING TEMPERATURE ON THE PROPERTIES OF POROUS MATERIALS FROM WASTE GLASS

ŠTUDIJ VPLIVA TEMPERATURE SINTRANJA NA LASTNOSTI POROZNIH MATERIALOV IZ ODPADNEGA STEKLA

Nguyen Vu Uyen Nhi[1,2], Do Quang Minh[1,2], Le Thi Quynh Anh[1,2], Kieu Do Trung Kien[1,2]*

[1]Faculty of Materials Technology, Ho Chi Minh City University of Technology (HCMUT), 268 Ly Thuong Kiet Street, District 10, Ho Chi Minh City, Vietnam
[2]Vietnam National University Ho Chi Minh City, Linh Trung Ward, Thu Duc City, Ho Chi Minh City, Vietnam

Prejem rokopisa – received: 2025-05-13; sprejem za objavo – accepted for publication: 2025-08-28

doi:10.17222/mit.2025.1453

The growing volume of environmental waste glass underscores the importance of recycling for sustainable development. A promising approach is the recycling of waste glass into porous materials. This study investigates the influence of sintering temperature on the properties of porous materials made from waste glass. Material samples were fabricated by adding liquid sodium silicate to glass powder at a glass powder/liquid sodium silicate ratio of 9/1. The optimal sintering temperature range for the porous material was determined through a heating microscope, revealing a suitable range of 770–830 °C. The sintered porous glass samples were evaluated based on the properties such as pore size distribution, density, water absorption, and porosity of the product. Furthermore, Fourier transform infrared spectroscopy was employed to assess the functional group composition of the product. This research provides an effective recycling solution for waste glass by transforming it into porous materials with significant potential applications.

Keywords: waste glass, porous materials, heating microscope, recycled materials, sintering

Usmeritev v trajnostni razvoj zaradi globalnega segrevanja povečuje zahteve po ponovni predelavi (recikliranju) in uporabi vedno večjih količin odpadnega stekla. Obetaven pristop je recikliranje odpadnega stekla v porozne materiale. V tem članku avtorji opisujejo raziskavo vpliva temperature sintranja na lastnosti poroznih materialov izdelanih iz odpadnega stekla. Vzorce materiala so avtorji izdelali z dodatkom raztaljenega natrijevega silikata k odpadnemu steklenemu prahu v razmerju steklo/Na-silikat 9:1. Optimalno območje temperatur sintranja so avtorji določili s pomočjo ogrevalnega mikroskopa in ugotovili da se nahaja med 770 °C in 830 °C. Vzorce sintranega poroznega stekla so avtorji nato okarakterizirali. Določili so velikostno porazdelitev por, gostoto, absorpcijo vode in celokupno poroznost. Nadalje so s pomočjo Furierjeve Transformacijske Infrardeče spektroskopije (FTIR; angl.: Fourier Transform Infrared Spectroscopy) ocenili funkcionalno skupinsko sestavo sintranih vzorcev. Avtorji v zaključkih ugotavljajo, da so s pomočjo te raziskave predstavili in podali učinkovito rešitev za recikliranje odpadnega stekla z njegovo predelavo v porozni material, ki ima velike možnosti za nadaljnjo uporabo.

Ključne besede: odpadno steklo, porozni materiali, ogrevalni mikroskop, reciklirani materiali, sintranje

1 INTRODUCTION

Vietnam generates over 120,000 tons of glass waste annually, which is expected to rise with an ongoing population growth and urbanization. Unfortunately, with a recycling rate of only about 10 %, most of this material is sent to landfills. When landfilled, hazardous substances from the glass can leach into soil and water, contaminating water sources and impacting public health. Furthermore, discarded waste glass detracts from urban aesthetics, affecting the landscape and quality of life. Therefore, developing methods to recycle this waste is crucial for protecting the environment, conserving resources, and reducing landfill pressure.

One promising route for recycling waste glass is its conversion into porous materials, which have wide-ranging applications in construction, water treatment, and insulation. While several fabrication methods exist, chemical routes involving sintering with foaming agents[1–4] or binders are most common for glass-based materials.[5,6] Previous studies have demonstrated the feasibility of using additives such as $CaCO_3$ or sodium silicate (liquid glass) to induce a porous structure during thermal processing. Among these, sodium silicate is recognized as a particularly effective and low-cost additive.

Following this research direction, B. K. Thach et al. investigated a process for recycling waste glass from photovoltaic panels to produce porous glass materials. The study focused on incorporating $CaCO_3$ and liquid glass with waste glass to form a porous structure. The sintering process was carried out within a temperature range of 830–910 °C, with key thermal parameters determined using a heating microscope.[7] Pat Sooksaen et al.

*Corresponding author's e-mail:
kieudotrungkien@hcmut.edu.vn (Kieu Do Trung Kien)

studied a process for fabricating lightweight glass foam with applications in thermal insulation, using finely ground glass powder from waste glass bottles as the primary raw material. In this process, sodium silicate was used as the binder, while yellow glycerol and sodium carbonate served as foaming agents, forming the material's porous structure.[8] Seun Samuel et al. synthesized glass foam from waste glass, using liquid glass as the foaming agent. The study utilized different glass particle sizes and performed sintering at 800 °C and 850 °C. The results showed that the glass foam's porosity increased proportionally with temperature and particle size.[9]

The studies above demonstrated that waste glass needs to be mixed with a supporting additive and sintered at the melting temperature of the glass to create porosity. Sodium silicate can be considered an effective and low-cost option among various supporting additives. Despite the established efficacy of sodium silicate in pore formation, a systematic investigation into the influence of sintering temperature on the final microstructural and physical properties of the resulting material remains limited in the existing literature. This knowledge gap is significant, as the thermal conditions within the glass softening range are paramount to controlling pore development,[10] yet this process-property relationship has not been thoroughly elucidated.[10]

Therefore, the primary objective of this study is to systematically investigate the effect of sintering temperature within a range of 770–830 °C, on the properties of porous materials fabricated from waste glass using sodium silicate as the binder. Key characteristics are thoroughly analyzed, including bulk density, water absorption, total and open porosity, and pore size distribution. The goal is to establish a relationship between the processing temperature and the material's final properties, providing a scientific basis for process optimization and future applications.

2 EXPERIMENTAL PART

2.1 Materials

Waste glass was sourced from Thien Phu Co., Ltd. It originated from processing flat glass sheets used in construction applications. Glass powder was collected and milled in a high-energy ball mill for 15 min. Each batch had a mass of 250 g. The chemical composition of the waste glass was determined by X-ray fluorescence. The mineralogical composition was determined by X-ray diffraction.

In addition to waste glass, liquid sodium silicate was the supporting material for the pore formation. Sodium silicate was obtained from Central Chemical Supplies. Its chemical formula is $Na_2O{\cdot}nSiO_2{\cdot}mH_2O$. It exhibited a density of 1.38 g/cm^3.

2.2 Methods

The research process flowchart is depicted in **Figure 1**. Waste glass, after milling, was analyzed by X-ray fluorescence, X-ray diffraction, and Fourier transform infrared spectroscopy to assess the properties of the raw material. Subsequently, waste glass was mixed with liquid glass at a waste glass/liquid glass mass ratio of 9/1. Additionally, water was added at 20 % by mass of waste glass to improve the formability of the samples. After thorough mixing to achieve a homogeneous mixture, the blend was poured into molds with a diameter of 42 mm and a height of 18 mm and then dried to remove moisture. After that, the samples were sintered at different temperatures and a heating rate of 3 °C/min. The dwell time at the maximum temperature was 4 h to promote pore formation. Finally the samples were cooled rapidly to room temperature. The sintering temperature range was determined using a heating microscope. The sintered samples were then subjected to measurements of their physical properties and pore size distribution to evaluate

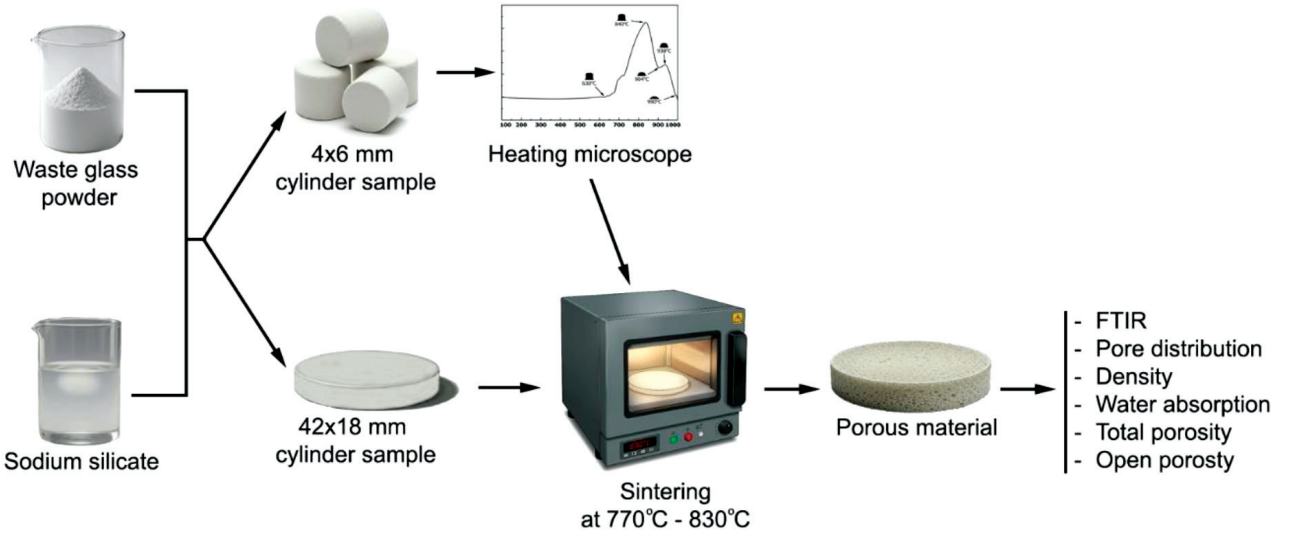

Figure 1: Research process flowchart

Table 1: Summary of characterization techniques and parameters

Analysis technique	Instrument/ standard	Purpose	Key parameters / sample form
X-ray fluorescence	Thermo ARL ADVANT'X	To determine the chemical composition of the raw waste glass	Powder sample
X-ray diffraction	D2 PHASER (Bruker)	To identify the crystalline phases present in the waste glass	Cu-K_α radiation (λ = 0.15418 nm), 2θ range: 10–80°, step size: 0.026°
Fourier transform infrared spectroscopy	NICOLET 6700	To identify the functional groups in the raw and sintered materials	Wavenumber range: 4000–480 cm^{-1}, mixed with KBr to form pellets
Heating microscopy	EM 201 (Hesse Instrument)	To observe the thermal behavior (softening, sintering) and determine the optimal sintering temperature range	Cylindrical sample (H = 6 mm, D = 4 mm); heating rate: 3 °C/min
Physical property measurement	ASTM C20-00 standard	To quantify bulk density, water absorption, total porosity, and open porosity	Measurements conducted according to the standard's procedures
Pore structure analysis	ImageJ software	To analyze the pore size and distribution from sample images	Analysis performed on digital images of the sintered sample surfaces

the effectiveness of the process for producing porous materials from waste glass. For physical properties, three separate samples were prepared and tested to ensure the reproducibility of the results. The physical property data presented herein include mean values, with error bars indicating the standard deviation.

2.3 Analysis methods

The chemical compositions of waste glass were analyzed using X-ray fluorescence (XRF) to assess purity. The analysis was performed using a Thermo ARL ADVANT'X instrument on 10 g powder samples.

The functional group composition of a sample was determined using Fourier transform infrared spectroscopy (FTIR) with a NICOLET 6700 instrument (Thermo Scientific). Samples were prepared as fine powders and mixed with KBr to form pellets. FTIR spectra were recorded in the transmission mode over a wavenumber range of 4000–480 cm^{-1}, with a spectral resolution of 0.21 cm^{-1}. Characteristic absorption peaks in the FTIR spectra were analyzed to identify the presence of functional groups in the samples.

The phase composition of waste glass was determined using X-ray diffraction (XRD) with a D2 PHASER instrument (Bruker). XRD patterns were recorded in the reflection mode, using Cu-Kα radiation (λ = 0.15418 nm), over a 2θ range of 10–80° with a step size of 0.026°. Samples were prepared as fine powders. Diffraction peaks in the XRD patterns were used to identify the crystalline phases present in the waste glass.

A heating microscope (HM) was used to observe the thermal behavior of the pellet samples during heating. From this, characteristic temperatures of the material were determined. An HM analysis was performed using an EM 201 instrument (Hesse Instrument). The samples were cylindrical, with dimensions of H = 6 mm and D = 4 mm. The sample holder was made of steel, conforming to the DIN 51730 standard. The samples were heated at a rate of 3 °C/min.

The shape, size, and distribution of pores were analyzed using digital images of the material. These parameters were quantified using ImageJ software. The physical properties of the samples, such as bulk density, water absorption, total porosity, and open porosity, were determined according to the ASTM C20-00 standard.

Analytical methods are summarized in **Table 1**.

3 RESULTS AND DISCUSSION

3.1 Characterization of waste glass raw material

The chemical composition of waste glass was determined using the XRF analysis. The results are presented in **Table 2**.

Table 2: Chemical composition of waste glass (*w*/%)

SiO_2	CaO	Na_2O	MgO	Al_2O_3	K_2O	Others	L.o.I(*)
53.49	9.25	8.05	2.65	0.96	0.34	0.5	22.47

(*) L.o.I – loss on ignition

The chemical composition analysis revealed that a waste glass sample primarily consists of SiO_2 (53.49 *w*/%). SiO_2 is the main component in the glass structure. Typically, the SiO_2 content in glass ranges from 70–73 %.[11,12] A reduced SiO_2 content is attributed to impurities incorporated into glass during processing and storage. These impurities prevent glass from being reused via a glass melting process. Therefore, alternative treatment methods are required for this type of glass. Besides SiO_2, the loss of ignition (L.o.I.) content of 22.47 *w*/%, is also a significant component in the waste glass. L.o.I. represents the volatile components of a sample that are released upon heating up to 950 °C. Specifically, a temperature range of 300–600 °C corresponds to the decomposition of organic compounds, while a range of 600–950 °C corresponds to the decomposition of carbonates. A high L.o.I. value suggests that a significant gas is generated during sintering. This phenomenon is fundamental to creating porous materials from this glass source. When sintered at an appropriate temperature, the high viscosity of molten glass traps this gas, forming a porous structure.

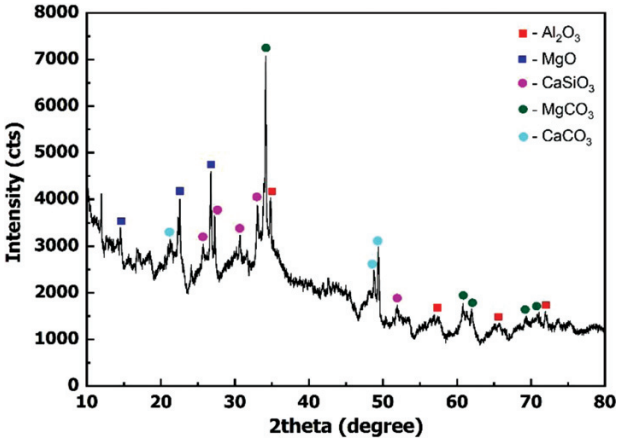

Figure 2: XRD pattern of the waste glass

The mineralogical composition of the waste glass, as determined by the XRD analysis, is presented in **Figure 2**. The XRD pattern in this figure shows that the sample contains the following main crystalline phases: Al_2O_3, MgO, $CaSiO_3$, $MgCO_3$, and $CaCO_3$. The Al_2O_3 crystalline phase is indicated by diffraction peaks at 2θ values of 34.79°, 57.40°, 65.64°, and 71.92°.[13,14] The MgO crystalline phase exhibits diffraction peaks at 2θ values of 14.51°, 22.58°, and 26.75°.[15] The $CaSiO_3$ crystalline phase is represented by diffraction peaks at 2θ values of 25.70°, 27.28°, 30.69°, 33.11°, and 51.91°.[16] $MgCO_3$ is indicated by peaks at 2θ values of 34.16°, 60.79°, 62.02°, 69.35°, and 70.84°.[17] $CaCO_3$ is presented by peaks at 2θ values of 21.29°, 48.76°, and 49.39°.[18] These crystalline phases are impurities incorporated into the waste glass during processing and storage. These components render waste glass unsuitable for reuse in glass manufacturing. In addition to the crystalline impurity phases, the XRD pattern reveals a weak amorphous phase. This weak amorphous phase is characteristic of the waste glass component.

The functional group composition of the waste glass was also assessed using FTIR. **Figure 3** shows the FTIR spectrum of a waste glass sample. The results indicate the presence of the following functional groups in the waste glass: -OH at a wavenumber of 3473 cm^{-1},[19] C-H_n at wavenumbers of 2933 cm^{-1} and 2865 cm^{-1} [20,21], C=C at a wavenumber of 1652 cm^{-1} [22,23], CO_3^{2-} at a wavenumber of 1433 cm^{-1},[24] Al-O at a wavenumber of 1027 cm^{-1} [25], Si-O at wavenumbers of 788 cm^{-1} and 655 cm^{-1} [26,27], and Mg-O, Ca-O at a wavenumber of 453 cm^{-1}.[28,29] These functional groups are consistent with the results of the XRD analysis. The results once again confirm the presence of impurities related to Al_2O_3, $CaSiO_3$, MgO, $CaCO_3$, and $MgCO_3$ in the sample. Additionally, functional groups associated with C-H_n and C=C indicate the presence of certain organic compounds in waste glass. These organic compounds, along with $CaCO_3$ and $MgCO_3$, decompose and release gases at high temperatures. This is the reason for the high L.o.I. value observed in the chemical composition of the waste glass in **Table 2**.

Based on the results of the chemical composition and phase composition analyses, it is evident that waste glass can be effectively utilized as a primary raw material for the fabrication of porous materials. The loss-of-ignition component of waste glass, comprising organic impurities and carbonate compounds, can release gases during sintering. Meanwhile, the high-viscosity glass phase can trap the released gas bubbles, forming a porous material.

3.2 Determining the sintering temperature

HM was employed to determine the appropriate sintering temperature range. Test samples were prepared from a mixture of waste glass and liquid glass (at a 9:1 mass ratio), with water added at 20 % by mass of the waste glass to enhance formability. After thorough mixing, the mixture was shaped into cylindrical pellets with a diameter of 4 mm and a height of 6 mm. **Figure 4** presents the results of the HM analysis. They indicate that the changes in a sample's shape can be divided into three stages corresponding to different temperature ranges:

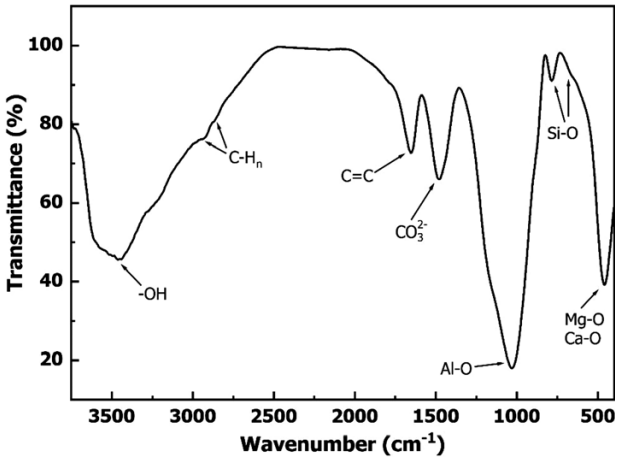

Figure 3: FTIR spectrum of the waste glass

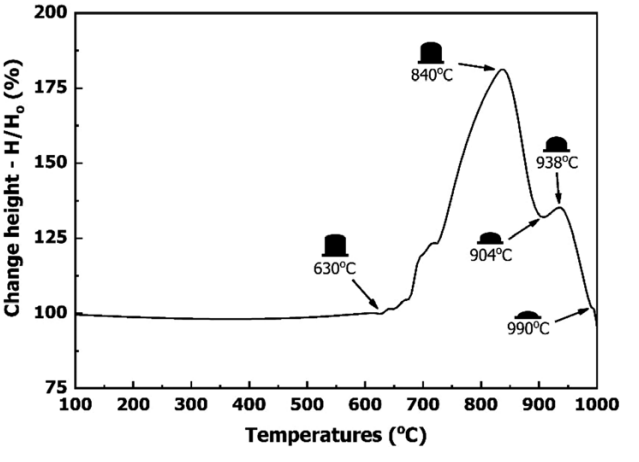

Figure 4: Analysis of the deformation of the sample height with respect to temperature

Stage 1 corresponds to a temperature range of 100–630 °C. During this stage, the decomposition of organic compounds occurs. However, since waste glass has not yet undergone significant physicochemical changes, the generated gas escapes from the sample through capillary pores. Therefore, the shape of the sample does not exhibit significant changes.

Stage 2 occurs within a temperature range of 630–840 °C. The sample undergoes significant deformation in this temperature range, characterized by increased volume. In studies related to thermal transformation processes, this temperature range corresponds to the final stage of organic compound decomposition and the initial stage of carbonate decomposition[17,30,31]. Carbonate minerals in the waste glass can be identified in **Figures 2** and **3**. The substantial increase in size during this stage indicates that this temperature range corresponds to the softening/melting of the glass. As it is softened, the viscosity of the glass is relatively high in this stage. As a result, the evolved gas cannot completely escape, thus contributing to the formation of a porous structure in the material. It should also be noted that, typically, construction glass has a melting temperature above 900 °C.[32] However, the addition of liquid glass helps lower the construction glass's softening temperature to approximately 630 °C.

Stage 3 corresponds to temperatures above 840 °C. Within this temperature range, the sample exhibits a significant decrease in size. During this stage, carbonate decomposition continues to occur. However, at these elevated temperatures, molten glass exhibits a low viscosity, which causes it to fill the existing pores and shrink the sample. Therefore, it can also be predicted that the porosity of the sample decreases during this stage. Within the temperature range above 840 °C, there is a region between 904 °C and 938 °C where the sample shows a slight increase in size; this temperature range corresponds to intensified carbonate decomposition reactions. Nevertheless, the pore-forming effect is negligible compared to the pore-filling impact of the molten glass, so this temperature range is not selected for sintering waste glass into a porous material.

These results indicate that the 630–840 °C temperature range is optimal for producing porous glass. Notably, porosity is expected to increase significantly as the temperature approaches 840 °C. Consequently, temperatures of (770, 790, 810 and 830) °C were selected for a further analysis of the temperature's impact on the property of the porous material derived from waste glass.

3.3 Characterization of sintered porous material

Based on the material characterization and thermal behavior of the mixture, the shaped samples were sintered at temperatures of (770, 790, 810, and 830) °C to produce porous materials with varying properties. The sintered products were then characterized to evaluate different aspects of the material. **Figure 5** presents the results of the density and water-absorption analyses of the products.

The results in **Figure** 5 show that the bulk density of the samples decreases as the sintering temperature increases. The most significant decrease in bulk density occurs within a temperature range of 770–790 °C. The water-absorption measurements indicate that this material has high water-absorption capacity. Water absorption increases continuously over a temperature range of 770–830 °C, which is consistent with the decrease in bulk density of the samples. These results demonstrate that the sintering temperature significantly influences the porous structure of the material. This trend is governed by the interplay between gas generation and the temperature-dependent viscosity of the glass matrix. As the temperature rises, the decomposition of organic and carbonate compounds accelerates, increasing gas release. At lower temperatures like 770 °C, the glass viscosity is high, which traps the gas but constrains bubble expansion and merging. This results in smaller, less connected pores. As the temperature increases towards 830 °C, the viscosity of the molten glass decreases significantly. This lowered viscosity facilitates the expansion of individual gas bubbles and their coalescence into larger voids. This mechanism directly leads to an increase in the average pore size (**Figure 8**) and a more interconnected pore network, thus decreasing the material's bulk density and increasing its water-absorption capacity.

Changes in the material structure are shown by the FTIR analysis results for the samples sintered at different temperatures. **Figure 6** presents the FTIR spectra of the samples sintered at (770, 790, 810 and 830) °C. Comparing the results from **Figure 6** with the FTIR analysis of the waste-glass raw material from **Figure 3** reveals significant changes in the functional group composition of the product after sintering compared to the raw material. Functional groups such as Al-O, Si-O, Mg-O, and Ca-O are still found in the composition of the product. These bonds are associated with inorganic compounds that are stable at high sintering temperatures. Conversely,

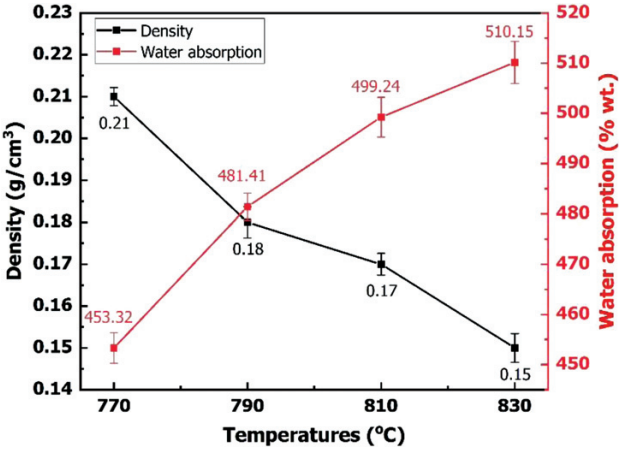

Figure 5: Density and water absorption of the samples

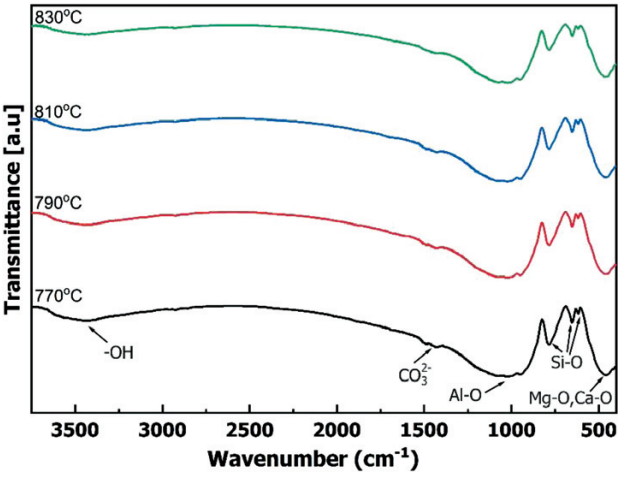

Figure 6: FTIR spectra of the samples

functional groups such as C-Hn and C=C, at wavenumbers of (2933, 2865 and 1652) cm^{-1}, are no longer observed in the FTIR analysis results of the product. Notably, the intensity of the characteristic peak for the CO_3^{2-} group at 1433 cm^{-1} is significantly decreased. This decrease becomes more pronounced with increasing sintering temperature. These results structurally demonstrate the thermal decomposition of organic compounds and carbonate compounds at elevated temperatures. This thermal decomposition contributes to the formation of pores in the product. Furthermore, the observed decrease in bulk density and increase in water absorption at sintering temperatures above 770 °C are primarily attributed to the continued decomposition of carbonate salts.

Changes in the pore structure of the material at different sintering temperatures can also be visually observed on digital images of the samples. Sample surfaces are shown in **Figure** 7. Visually, these images also demonstrate a successful creation of porous material from waste glass and liquid sodium silicate at sintering temperatures ranging from 770 °C to 830 °C. The higher sintering temperature altered the pore structure of the material. Specifically, the size of the pores increased, and the thickness of pore walls decreased. The pore size and pore-size distribution were measured and analyzed in detail using ImageJ software. **Figure 8** presents the results of the pore size distribution analysis of the samples using the software.

The pore size distribution analysis results in **Figure 8** show that the pore sizes vary from less than 1 mm to a maximum of approximately 7–8 mm, depending on the sintering temperature. The pore size distribution of the samples tends to be skewed to the left, indicating a greater number of smaller pores compared to larger ones. As the sintering temperature increases, the average pore size tends to increase. Specifically:

At a sintering temperature of 770 °C, the pores are most concentrated in the 1–2 mm range, with a significant number of pores being smaller than 1 mm. The number of pores decreases as the pore size increases.

At a sintering temperature of 790 °C, the pore size distribution is broader compared to that at 770 °C. The pores are most concentrated in the 2–3 mm range. Larger pores, exceeding 7 mm, also appear, although their number is still small.

At a sintering temperature of 810 °C, the pore size distribution is similar to that at 790 °C, but the peak is shifted towards larger sizes, indicating an increase in the distribution of larger pores. The number of pores smaller than 1 mm is also fewer compared to that at 770 °C.

At a sintering temperature of 830 °C, the pore size distribution is the broadest among the four temperatures. The peak of the distribution is significantly shifted towards larger sizes, indicating a substantial increase in the formation of large pores. Pores larger than 8 mm also appear, and the number of pores smaller than 1 mm is very small.

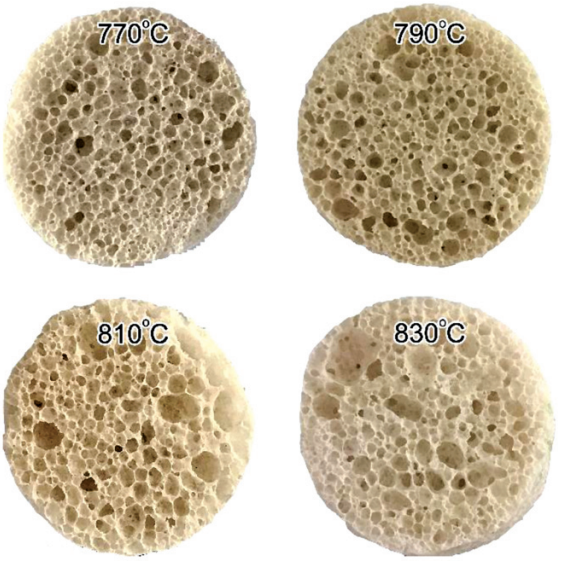

Figure 7: Surface morphologies of the samples after sintering

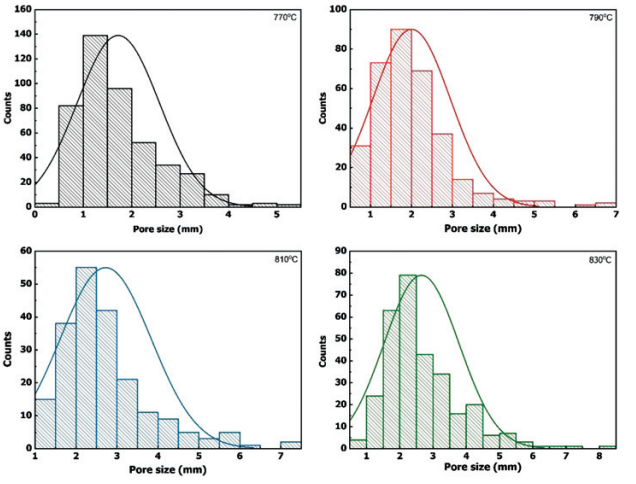

Figure 8: Pore-size distribution of the samples

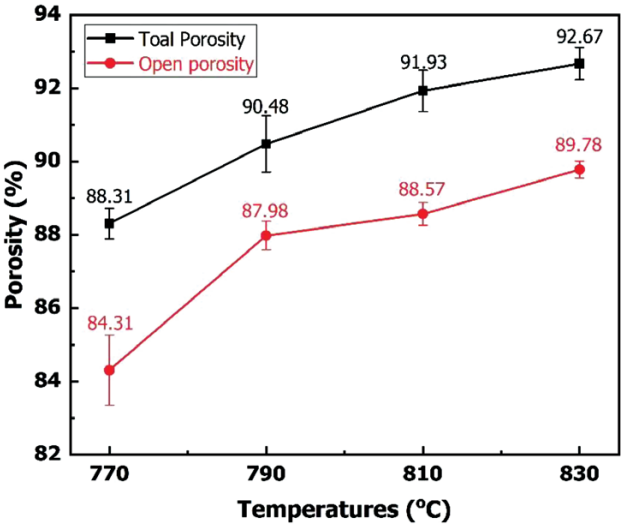

Figure 9: Influence of the sintering temperature on porosity

These results demonstrate that the sintering temperature directly influences the pore size and its distribution. Specifically, as the temperature rises, the average pore size and breadth of the distribution increase. This trend can be attributed to enhancing processes like particle coalescence and volatilization of pore-forming agents at elevated temperatures. The pores also tend to coalesce, creating larger pores and reducing the number of smaller pores.

Besides the pore size distribution, the relationship between open porosity and total porosity was also determined according to the ASTM C20-00 standard. **Figure 9** analyses the relationship between open and total porosity in the samples. The results show that both total and open porosity increase with increasing sintering temperature. However, the increase in open porosity is more pronounced than in total porosity. This suggests that higher temperatures may promote the formation or expansion of pores within the material. As a result, more interconnected pores are formed. The correlation between total and open porosity also indicates that open porosity is the dominant component in the pore structure. In particular, the rapid increase in open porosity in the temperature range of 770–790 °C, and the slower increase between 790 °C and 830 °C further suggest that the reduced viscosity of the liquid phase at higher temperatures also reduces the rate of open pore development in the material. Overall, this material exhibits high porosity, making it a promising candidate for applications such as filtration, adsorption, sound and thermal insulation, catalysis, or as a support material.

The observed trend of increasing porosity with temperature is consistent with the findings of Owoeye et al. relating to similar foam glass materials.[9] However, the novelty of the present study lies in its systematic analysis across a narrow and critical temperature range, allowing for a detailed characterization of the pore architecture. The achievement of over 92 % total porosity and nearly 90 % open porosity highlights the effectiveness of this process. This high degree of interconnectivity is a key contribution, suggesting strong potential for applications like filtration or catalyst support, which rely on permeable structures.

4 CONCLUSIONS

This study successfully demonstrated the fabrication of highly porous materials from waste glass using sodium silicate as the binder, with sintering temperature emerging as the critical control parameter. The investigation confirmed that increasing the sintering temperature from 770 °C to 830 °C enhanced the material's porosity. The results showed that the bulk density significantly decreased from 0.21 to 0.15 g/cm^3, while the total porosity rose to an exceptionally high 92.67 % at the optimal temperature of 830 °C. Most significantly, the open porosity reached 89.78 %, indicating a highly interconnected pore network, which was further confirmed by an increase in the average pore size up to 8 mm. The high degree of open porosity makes this material a promising candidate for applications in filtration, absorption, and catalyst support. Future research should focus on quantifying the material's mechanical properties, including compressive strength, and assess its application-based performance through key metrics such as filtration efficiency and thermal conductivity.

Acknowledgment

This research is funded by the Vietnam National University Ho Chi Minh City under grant number C2024 – 20 – 22. We acknowledge the Ho Chi Minh City University of Technology (HCMUT), VNU – HCM for supporting this study.

5 REFERENCES

[1] J. Rouquerol, D. Avnir, C. W. Fairbridge, D. H. Everett, J. M. Maynes, N. Pernicone, J. D. F. Ramsay, K. S. W. Sing, K. K. Unger, Recommendations for the characterization of porous solids, Pure Appl. Chem., 66 (**1994**), 1739–1758, doi:10.1351/pac199466081739

[2] E. Samson, J. Marchand, J. Beaudoin, Modeling the influence of chemical reactions on the mechanisms of ionic transport in porous materials: an overview, Cem. Concr. Res., 30 (**2000**), 1895–1902, doi:10.1016/S0008-8846(00)00458-0

[3] A. Vu, Y. Qian, A. Stein, Porous Electrode Materials for Lithium-Ion Batteries – How to Prepare Them and What Makes Them Special, Adv. Energy Mater., 2 (**2012**), 1056–1085, doi:10.1002/aenm.201200320

[4] E. Mercadelli, C. Galassi, How to Make Porous Piezoelectrics? Review on Processing Strategies, IEEE Trans. Ultrason. Eng., 68 (**2021**), 217–228, doi:10.1109/TUFFC.2020.3006248

[5] D. Bajare, G. Bumanis, A. Korjakins, New porous material made from industrial and municipal waste for building application, Mater. Sci., 20 (**2014**), 333–338, doi:10.5755/j01.ms.20.3.4330

[6] T. Takei, H. Ota, Q. Dong, A. Miura, Y. Yonesaki, N. Kumada, H. Takahashi, Preparation of porous material from waste bottle glass by

hydrothermal treatment, Ceram. Int., 38 (**2012**), 2153–2157, doi:10.1016/j.ceramint.2011.10.057

[7] B. K. Thach, L. N. Tan, D. Q. Minh, L. C. Hung, P. D. Tuan, Production of Porous Glass-Foam Materials from Photovoltaic Panel Waste Glass, Proceedings of the Green Materials and Electronic Packaging Interconnect Technology Symposium, 2012, 317–327, doi:10.1007/978-981-19-9267-4_34

[8] P. Sooksaen, N. Sudyod, N. Thongtha, R. Simsomboonphol, Fabrication of lightweight foam glasses for thermal insulation applications, Mater. Today: Proc., 17 (**2019**), 1823–1830, doi:10.1016/j.matpr.2019.06.219

[9] S. S. Owoeye, G. O. Matthew, F. O. Ovienmhanda, S. O. Tunmilayo, Preparation and characterization of foam glass from waste container glasses and water glass for application in thermal insulations, Ceram. Int., 46 (**2020**), 11770–11775, doi:10.1016/j.ceramint.2020.01.211

[10] J. H. Kim, M. Kim, J.-S. Yu, Recycle of silicate waste into mesoporous materials, Environ. Sci. Technol., 45 (**2011**), 3695–3701, doi:10.1021/es103510r

[11] D. R. Liu, J. S. Park, R. E. Benoit, F. D. Jackson, Chemical analysis of ream defect in float glass, X-Ray Spectrom., 21 (1992), 293–298, doi:10.1002/xrs.1300210607

[12] A. Iatsenko, A. Mishchenko, B. Kornilovych, The effect of nano-silica and waste glass powder on mechanical, rheological, and shrinkage properties of UHPC using response surface methodology, J. Mater. Res. Technol., 8 (**2019**), 804–811, doi:10.1016/j.jmrt.2018.06.011

[13] A. A. Mohammed, Z. T. Khodair, A. A. Khadom, Preparation and investigation of the structural properties of α-Al_2O_3 nanoparticles using the sol-gel method, Chem. Data Collect., 29 (**2020**), 100531, doi:10.1016/j.cdc.2020.100531

[14] K. D. T. Kien, L. M. Son, D. Q. Minh, T. Q. Nhat, Development of refractory concrete using glass grinding waste sand, Mater. Technol., 58 (**2024**), 737–743, doi:10.17222/mit.2024.1263

[15] I. W. Sutapa, A. W. Wahab, P. Taba, N. La Nafie, Synthesis and structural profile analysis of the MgO nanoparticles produced through the sol-gel method followed by annealing process, Orient. J. Chem., 34 (**2018**), 1016, doi:10.13005/ojc/340252

[16] D. Li, H. Wang, Z. He, Z. Xiao, R. Lei, S. Xu, Effect of CuO addition on the sintering temperature and microwave dielectric properties of $CaSiO_3$–Al_2O_3 ceramics, Prog. Nat. Sci.: Mater. Int., 24 (**2014**), 274–279, doi:10.1016/j.pnsc.2014.04.003

[17] S. B. Choi, N. W. Kim, D. K. Lee, H. Yu, Growth mechanism of cubic MgO granule via common ion effect, J. Nanosci. Nanotechnol., 13 (**2013**), 7577–7580, doi:10.1166/jnn.2013.7882

[18] M. Seifan, A. Khajeh Samani, S. Hewitt, A. Berenjian, The effect of cell immobilization by calcium alginate on bacterially induced calcium carbonate precipitation, Fermentation, 3 (**2017**), 57, doi:10.3390/fermentation3040057

[19] D. Luo, Y. Lei, N. Zhao, H. He, K. Abrar, K. Li, Unique Double Carbon Protection Structured Co_3O_4 Anode for Lithium Ion Battery, J. Mater. Sci. Chem. Eng., 8 (**2020**), 56, doi:10.4236/msce.2020.812005

[20] K. D. T. Kien, P. D. Tuan, T. Okabe, D. Q. Minh, T. Khai, Study on sintering process of woodceramics from the cashew nutshell waste, J. Ceram. Process. Res., 19 (**2018**), 472–478, doi:10.36410/jcpr.2018.19.6.472

[21] M. Kurečič, M. Sfiligoj-Smole, K. Stana-Kleinschek, UV Polymerization of poly (N-Isopropylacrylamide) hudrogel, Mater. Technol., 46 (**2012**), 87–91

[22] T. Van Khai, H. N. Minh, N. V. U. Nhi, K. D. T. Kien, Effect of composition on the ability to form SiC/SiO_2-C composite from rice husk and silica gel, J. Ceram. Process. Res., 22 (**2021**), 246–251, doi:10.36410/jcpr.2021.22.2.246

[23] S. Sugiman, P. D. Setyawan, M. Maryudi, S. Madnasri, Water absorption, tensile, flexural and impact properties of aged bamboo fibre/nano $CaCO_3$-modified unsaturated polyester composites, J. Appl. Sci. Eng., 24 (**2021**), 239–251, doi:10.6180/jase.202104_24(2).0013

[24] T. Jiang, C. Wang, M. Chen, H. Hu, J. Huang, X. Chen, Q. Zang, Mechanochemical Synthesis of Dolomite-Related Carbonates—Insight into the Effects of Various Parameters, Miner., 13 (**2023**), 1359, doi:10.3390/min13111359

[25] N. Damayanti, Preparation of superhydrophobic PET fabric from Al_2O_3–SiO_2 hybrid: Geometrical approach to create high contact angle surface from low contact angle materials, J. Sol-Gel Sci. Technol., 56 (**2010**), 47–52, doi:10.1007/s10971-010-2271-0

[26] A. Samy, A. Ismail, H. Ali, Environmentally friendly mesoporous SiO_2 with mixed fiber/particle morphology and large surface area for enhanced dye adsorption, J. Mater. Sci., 58 (**2023**), 1586–1607, doi:10.1007/s10853-022-08119-2

[27] N. Ramlan, S. I. Zubairi, M. Y. Maskat, Response surface optimisation of polydimethylsiloxane (PDMS) on borosilicate glass and stainless steel (SS316) to increase hydrophobicity, Mol., 27 (**2022**), 3388, doi:10.3390/molecules27113388

[28] D. Durgalakshmi, R. Ajay Rakkesh, S. Kamil, S. Karthikeyan, S. Balakumar, Rapid dilapidation of alcohol using magnesium oxide and magnesium aspartate based nanostructures: A Raman spectroscopic and molecular simulation approach, J. Inorg. Organomet. Polym. Mater., 29 (**2019**), 1390–1399, doi:10.1007/s10904-019-01105-3

[29] M. Keshavarz, R. Foroutan, F. Papari, L. Bulgariu, H. Esmaeili, Synthesis of CaO/Fe_2O_3 nanocomposite as an efficient nanoadsorbent for the treatment of wastewater containing Cr (III), Sep. Sci. Technol., 56 (**2021**), 1328–1341, doi:10.1080/01496395.2020.1778727

[30] K. D. T. Kien, N. V. U. Nhi, Effect of Mg/ Cu additives on the ability to synthesize SiC from rice husk. J. Appl. Sci. Eng., 28 (**2024**), 1717–1726, doi:10.6180/jase.202508_28(8).0009

[31] M. Liu, M. Kang, K. Chen, Y. Mou, R. Sun, Synthesis and luminescent properties of $CaCO_3$: Eu^{3+}@SiO_2 phosphors with core–shell structure, Appl. Phys. A., 124 (**2018**), 1–10, doi:10.1007/s00339-018-1668-4

[32] R. Yu, The application of waste float glass, recycled in structural beams made with the glass casting method, Challenging Glass Conference Proceedings, 7 (**2020**), doi:10.7480/cgc.7.4775